Control of a New Swimming Microrobot Design Using Flatness-ANFIS-Based Approach

M. Meguellati, F. Srairi, F. Djeffal and L. Saidi

Abstract— **In this work, an analytical investigation-based framework is presented to study a new swimming microrobot design. The proposed analytical analysis is carried out by solving the coupled elastic/fluidic equations basing on the dynamic microcantilever tail, which is strongly affected by a joint fabricated by polymer ionic technique. The use of the Flatness-ANFIS based control represents an excellent approach in order to overcome the control and modeling limitations imposed by the system complexity. Our proposed control approach is based on the coupling between the differential flatness and adaptive neuro-fuzzy inference (ANFIS) technique. The use of the flatness technique allows the generation of the flat output. This latter improves the control strategy by including the real behavior of the swimming microrobot in a fluid environment. In addition, the neuro-fuzzy inference technique decreases the impact of the dynamic nonlinear effect on the swimming microrobot behavior.**

Index Terms— **ANFIS, Fuzzy computation, IPCM, Flatness, Control, Microrobotics, Swimming.**

I. INTRODUCTION

Nowadays, the microrobots take the lion's share of the different research fields of interest. They are increasingly important necessities for precision applications due to their speed in terms of response time and controllability in dangerous environments [1-6]. The surgical assistance microrobots are regularly used in operating rooms. Currently, the researchers have developed miniature endoscopic capsule robot able to explore intestinal conduits, arteries or veins, for assist the surgeon in his diagnosis, based on the entirety of submicron embedded sensors [7,8], or in military applications such as the description of the nuclear area or define a large moving targets [9-13].

Recently, many researches and practices are developed including new materials and design aspects [1-5]. Most of these microrobots used a huge number of parts, which leads to microrobot behavior degradation in terms of complexity and fabrication cost. In other hand, several investigations have been conducted on microrobot systems, which are not based on the biomimetic philosophy. New method was introduced by Chang et al [1], in this method; an external magnetic field is applied to rotate a small ferromagnetic screw in the liquid. However, speed limitation is the main disadvantage of this microrobot.

In this paper, we propose an analytical investigation based framework for the analysis of a new swimming microrobot design, which is compound by a spherical head and a hybrid flexible tail. Our modeling approach is analyzed by analytically solving the coupled elastic/fluidic problem, based-on the dynamic microcantilever tail strongly affected by a joint in polymer ionic. The IPMC system generally composites of perfluorinated polymers, such as sulfonated or carboxylated. Perfluorinated sulfonic acid ionomeric polymers are synthesized by copolymerization of sulfonyl fluoride vinyl ether and tetrafluoroethylene [14]. In addition, the initial motion which is provided by a magnetic field applied to the head of the microrobot increases the thrust force and ensures better performance in terms of stability, controllability and reliability of the microrobot device. Nowadays, the nonlinearity of control strategy presents the main concern of research in microrobotic-based applications. In fact, the ambiguous applications of the microrobot devices required fast and a high precision for control strategy, in order to get a high microrobot performance in terms of time responses and tracking errors. However, the majorities of the tasks entrusted to the microrobots are delicate and require a great precision in the hazardous trajectories. The use of the Flatness-ANFIS based control represents an excellent approach in this direction. Our control approach is based on the coupling between the differential flatness and adaptive neuro fuzzy inference (ANFIS) technique [15-16]. The use of the flatness technique allows us to generate flat output. This latter, pursuing the real behavior of the swimming microrobot in a fluid environment. In other hand, the neuro fuzzy inference technique ensures the decreasing of the effects of nonlinear system varying in time.

II. PRINCIPE OF THE MODELING

The structure of the investigated microrobot is illustrated in figure 1. As it is shown from this figure, our microrobot design is compound by a spherical head and a hybrid flexible tail. The tail has two IPCM joints and two passive plates as links. The plates are assumed to be rigid but thin and light. The volume of the head is considered as a vacuum sphere for placed the coil, drugs and sensors. The coil occupies 60% to provide the initial driving force, and the remainder 40% of the volume reserved for drugs and sensors.

m. meguellati is with the Department of Electronics, University of Batna, 05000, Algeria (e-mail: m_meguellati@ yahoo.fr).

F. Djeffal is with the Laboratory of Advanced Electronic, Department of Electronics, LEPCM, University of Batna, 05000, Algeria (e-mail: faycaldzdz@hotmail.com, faycal.djeffal@univ-batna.dz).

F. Srairi is with Department of Electronics, University of Batna, 05000, Algeria (e-mail:srairifawzi@yahoo.fr).

L. Saidi is with Department of Electronics, University of Batna, 05000, Algeria (e-mail:srairifawzi@yahoo.fr).

$$\vec{r} = i\,cos(\alpha) + j\,sin(\alpha)$$
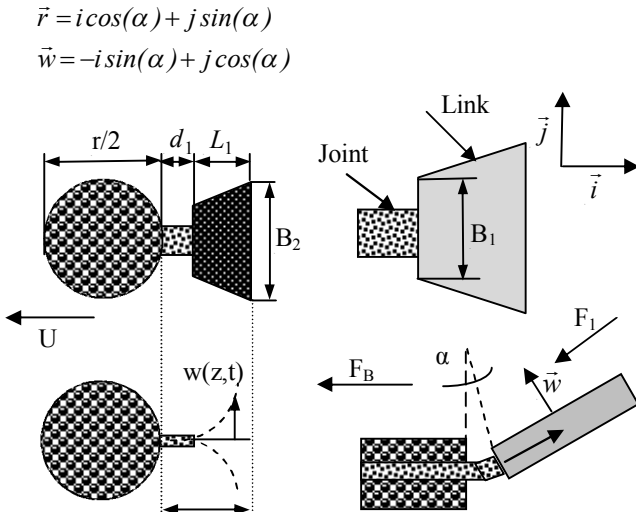$$\vec{w} = -i\,sin(\alpha) + j\,cos(\alpha)$$

Figure 1.   Cross sectional view of our proposed microrobot design with a description of the tail.

The governing equation for the dynamic deflection function $w(X,t)$ of the tail performing flexural oscillations is :

$$EI\frac{\partial^4 W(X,t)}{\partial X^4} + \mu\frac{\partial^2 W(X,t)}{\partial X^2} = F(X,t) \qquad (1)$$

where E presents the Young's modulus, I is the moment of inertial of the tail, μ is the mass per unit length of the Tail, F is the external applied force per unit length, x is the spatial coordinate along the length of the tail, and t is time. The boundary conditions of (1) are the usual clamped and free end conditions.

$$\left[W(x,t) = \frac{\partial W(X,t)}{\partial X} = \frac{\partial^2 W(X,t)}{\partial X^2} = \frac{\partial^3 W(X,t)}{\partial X^3} \right]_{X=0}$$
$$= \left[W(x,t) = \frac{\partial W(X,t)}{\partial X} = \frac{\partial^2 W(X,t)}{\partial X^2} = \frac{\partial^3 W(X,t)}{\partial X^3} \right]_{X=L,t=0} = 0$$

where L is the length of the tail (see Fig. 1). For a cantilever tail moving in a fluid, the external applied load $F(X,t)$ can be calculate as:

$$F(X,t) = -\rho_w\frac{\pi}{4}\Gamma(w)\ddot{a}\lambda_f\,sin(\alpha(t)) \qquad (3)$$

where ρ_w presents the density of fluid and $\Gamma(w)$ is the hydrodynamic function which is obtained from the solution of Navier Stokes Equation:

$$\nabla\hat{U} = 0, \; -\nabla\hat{P} + \eta\nabla^2\hat{U} = -iw\rho\hat{u}, \qquad (4)$$

Where $\hat{U}$ presents the velocity field, $\hat{P}$ is the pressure, ρ, η are the density and viscosity of the fluid, respectively.

Substituting (3) into (1) and rearranging we find:

$$\frac{\partial^2 W(X,t)}{\partial X^2} = a\frac{\partial^4 W(X,t)}{\partial X^4} + \frac{A}{EI}\ddot{a}\,sin(\alpha(t)) \qquad (5)$$

With $A = -\rho_w\frac{\pi}{4}\Gamma(w)\lambda_f$, $a = \frac{-\mu}{EI}$

Applying the above mentioned boundary conditions we obtained the following expression of 2-D tail's deflection $W(X,t)$:

$$W(X,t) = \left(-\frac{1}{2}w^2 + \frac{1}{4}Aw^2\right)t^2 + \left(-0.1819\,a + 3.9 + 45.4458\right)t$$
$$- 0.0249\,X^2 + \left(-0.0032\,a + 6.7284\right)X - \frac{1}{8}A\,cos(\,2tw\,) + \left(47.8928\,a^3\right)$$
$$\left(\frac{1}{a.94948}\right)Exp\left(45.6207 - \frac{1}{a}(X + 6.7543.t)\right) - 0.6728\,Xt + \frac{1}{8}A$$
$$- \left(a^2.4.8048.10^{-4}\right) - \left(a^2.2.3930.10^{-5}\right) + 7.6361.10^5$$

The lateral velocity of the tail can be calculated using 2-D tail's deflection $W(X, t)$, as:

$$U = \left[\sqrt{\frac{m\left(\frac{\partial w(z,t)}{\partial t}\right)^2}{C_D\rho_w S + m\left(\frac{\partial w(z,t)}{\partial z}\right)^2}} \right] \qquad (7)$$

The expression of Thrust force F_D is given by:

$$F_D = \frac{C_D\rho_w U^2 S}{2} + \tau_m V\|M\|B \qquad (8)$$

where τ_m is the magnetic ratio, m is the virtual mass density at $z=L$ expressed as $m = \frac{1}{4}\pi S_c^2\rho_w$, with Sc presents the width of the tail at the end $z=L$, S and C_D are the wetted surface area and drag coefficient, respectively.

III.   FLATNESS-ANFIS BASED CONTROL OF THE MICROROBOT DESIGN

The feedforward controller is designed based on the flatness input's method. The flatness based controller produce a flat input according to the given output signal which is work on the controlled plant. The structure chart of our microrobot with ANFIS-flatness control is shown in Fig. 2.
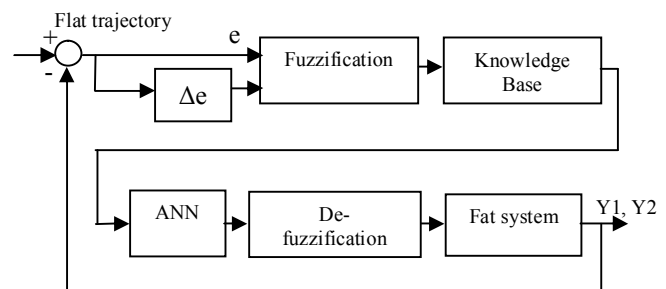

Figure 2.   Flowchart of our proposed Flatness-ANFIS-based control.

A.   Model of the microrobot

In this section we present the forces acting on our microrobot in fluid environment. So, the translational motion of the microrobot is expressed by:

$$\begin{cases} \ddot{X} = U_1\,sin(\theta) + U_2\,cos(\theta) + F_{dx} \\ \ddot{Z} = U_1\,cos(\theta) + U_2\,sin(\theta) - P + F_{dz} \\ \ddot{\theta} = \lambda U_2 \end{cases} \text{With} \begin{cases} U_1 = \frac{F_1}{m}cos(\alpha) \\ U_2 = -\frac{F_B}{m} \\ \lambda = \frac{mL_1}{J} \end{cases} \qquad (9)$$

where F_d is the drag force and equal to $F_d = -6\pi\eta r U$, $\vec{P} = \dfrac{V(\rho - \rho_f)\vec{g}}{m}$, V represents the total volume of the microrobot, ρ is the density mass, g is the vector of the gravity's acceleration, j is the moment of inertia. The geometrical and electomechanical configuration of the simulated microrobot is given in table 1.

TABLE I.　　MICROROBOT DESIGN AND SIMULATION PARAMETERS.

Parameter	Value
Blood density	1060 [Kg m^{-3}]
Magnetic material density	7874 [Kg m^{-3}]
Magnetization	1.72 .10^6 [Am^{-1}]
Yung's modulo	10^9 [Pa]
Blood velocity	0.025 [m.s^{-1}]
Robot's Radius	3 [µm]
Tail Length	4.10^{-3} [µm]
Magnetic ratio	0.8

B. Flatness-based control

By choosing the flat output $Y_1 = X - \dfrac{1}{\lambda}sin(\theta)$, $Y_2 = Z + \dfrac{1}{\lambda}cos(\theta)$, the flatness-based feedforward controller becomes

$$
\begin{cases}
X = Y_1 + \dfrac{1}{\lambda}\dfrac{\ddot{Y_1}}{\sqrt{(\ddot{Y_1})^2 + (\ddot{Y_2}+P)^2}} \\[2mm]
Z = Y_2 + \dfrac{1}{\lambda}\dfrac{\ddot{Y_2}+g}{\sqrt{(\ddot{Y_1})^2 + (\ddot{Y_2}+P)^2}} \\[2mm]
\theta = arctg\left(\dfrac{\ddot{Y_1}}{\ddot{Y_2}+g}\right) \\[2mm]
U_1 = -\dfrac{d^2}{dt^2}\left(Y_1 + \dfrac{1}{\lambda}\dfrac{\ddot{Y_1}}{\sqrt{(\ddot{Y_1})^2+(\ddot{Y_2}+P)^2}}\right)\left(\dfrac{\ddot{Y_1}}{\sqrt{(\ddot{Y_1})^2+(\ddot{Y_2}+P)^2}}\right) \\[2mm]
\quad + \dfrac{d^2}{dt^2}\left[\left(Y_2 - \dfrac{1}{\lambda}\dfrac{\ddot{Y_2}+g}{\sqrt{(\ddot{Y_1})^2+(\ddot{Y_2}+P)^2}}\right)+g\right]\left(\dfrac{\ddot{Y_2}+g}{\sqrt{(\ddot{Y_1})^2+(\ddot{Y_2}+P)^2}}\right) \\[2mm]
U_2 = \dfrac{1}{\lambda}\dfrac{d^2}{dt^2}\left(arctg\left(\dfrac{\ddot{Y_1}}{\ddot{Y_2}+P}\right)\right)
\end{cases}
\tag{10}
$$

C. Designing of ANFIS controller

The ANFIS structure considered as a multilayer feedforward network, which was proposed initially as a combination of fuzzy logic and artificial neural networks [15]. The ANFIS have both advantages of the neural network learning, capability and the structured knowledge representation employed in fuzzy inference systems. In the pioneer work of Jang [17-18], it is demonstrated that ANFIS is a universal competitive approximator compared to the most other existing approaches. In order to keep the microrobot in the desired trajectory, the strategy of the ANFIS control consists to adjust in permanent the values of the corrector gains. The neuro-fuzzy controller developed consists of two inputs, error (e) and change of error ($de = \dot{e}$) as it is shown in Fig. 3.
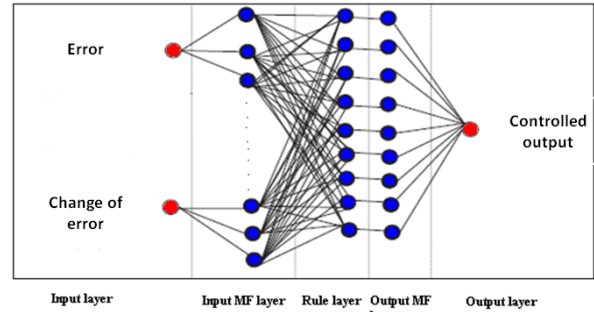

Figure 3.　Structure of ANFIS proposed for the microrobot's control with two inputs and one output.

The role of each layer of the network is described below:
- Layer 1: the output of each node gives the input variable membership grade.
- Layer 2: the firing strength associated with each rule is calculated.
- Layer 3: the calculation of the relative weight of each rule is achieved.
- Layer 4: the multiplication of normalized firing strength by first order of Sugeno fuzzy rule is realized.
- Layer 5: one node is composed and all inputs of the node are added up.

The inputs to the ANFIS controller which are the input error and the change in error are modeled by:

$$
\begin{aligned}
e(k) &= Y_{1,2\,Ref} - Y_{1,2} \\
\Delta e(k) &= e(k) - e(k-1)
\end{aligned}
\tag{11}
$$

The inputs of the fuzzy controller are error e and its variance ratio ec, and u is the output. The universe of fuzzy sets of e and u is {-1,-0.6,-0.2, 0, 0.2, 0.6, 1}, and the corresponding fuzzy sets is {NB, NM, NS, ZE, PS, PM, PB}. The universe of ec is {-1,-0.6,-0.2, 0, 0.2, 0.6, 1}, and its fuzzy sets is {NB, NM, NS, ZE, PS, PM, PB}. The fuzzy rules can be obtained by weighted average method. The fuzzy control rules are shown in Table. 1.

TABLE II.　　FUZZY CONTROL RULES.

E ＼ ΔE	NB	NM	NS	ZE	PS	PM	PB
NB	NB	NB	NB	NB	NM	NS	ZE
NM	NB	NB	NM	NM	NS	ZE	PS
NS	NB	NM	NS	NS	ZE	PS	PM
ZE	NB	NM	NS	ZE	PS	PM	PB
PS	NM	NS	ZE	PS	PS	PM	PB
PM	NS	ZE	PS	PM	PM	PB	PB
PB	ZE	PS	PM	PB	PB	PB	PB

IV. RESULTS AND DISCUSSION

In order to show the impact of our proposed design and to ensure the best control of our microrobot device, the flatness-ANFIS-based controller is investigated and developed, where the results will be compared to the conventional approaches. The typical data set should be stretching out as much as possible in the entire input-output space of data, in order to build an appropriate database for the ANFIS training set. The data set used for the training of our fuzzy system is obtained using the Matlab software. After the running of the learning algorithm, we find that the triangular function has higher rate of accuracy, where the recorded error for the training set equals to $3.1x10^{-3}$, which is the square mean error of tracking trajectory. It is to note that the number of epoch is set to 4000 and the method used for the train FIS is the back-propagation algorithm. The comparison between the generated results using different membership functions is investigated. The ANFIS response surface of the partition of the input/output variables using the best attained membership function is illustrated in figure. 4.

Figure. 5 illustrates the evolution of the thrust force F as a function of the radius of the microrobot's head. The curves are plotted assuming a gradient magnetic field 80 $mT.m^{-1}$. This latter ensures the magnetization of the microrobot to reach the saturation regime. Moreover, the thrust force is mainly depended to the magnetization of the microrobot's head. It is
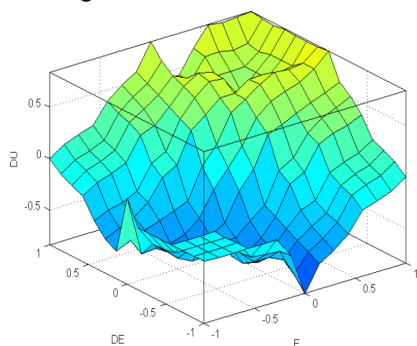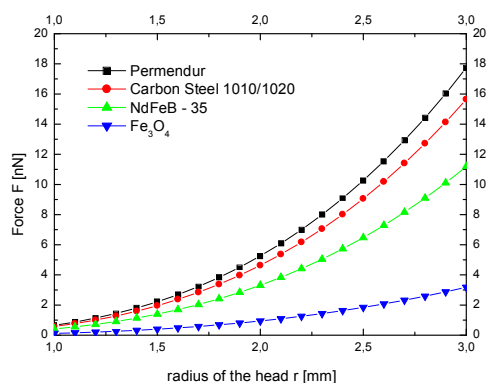
clear observed that the radius of the head is increased with the increase of the thrust force, and thus the controllability can be improved.

Figure. 6 shows the thrust force as a function of the length L and the width W of the tail compared with that of the conventional case. It is easy to note that when the values of the length and width are increased, the total thrust force can be increased. This result leads to improve the device performance compared to the conventional one. Therefore, our proposed design provides better performance in comparison to that given by the conventional structures, in terms of the thrust force, velocity and controllability of the swimming microrobot.

Figure .7 presents the behavior of the microrobot including the trajectory tracking parameter using the proposed ANFIS-based control. It is to note that an important tracking error value is recorded for $t=0s$ and $t=0.5s$. This period is considered as transition time, for which the device behavior should be improved. In this context, the obtained error is small than other published result [19]. Moreover, the recoded transition time provided by our control strategy is smaller than the recorded values given by conventional approaches, which means that our microrobot takes a short time to track the desired trajectory.
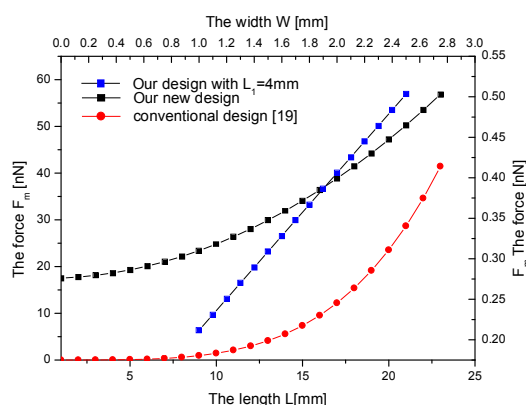

Figure 4.   ANFIS response surface.

Figure 6.   The thrust force in function of the length L and the width W of the tail compared with that of the conventional case.

Figure 5.   The thrust force F as a function of the radius of the head r for different magnetic materials.
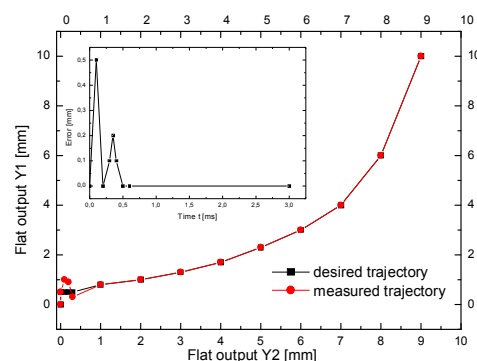

Figure 7.   The behavior of the microrobot in pursuit of the desired flat trajectory of the computed torque control by using ANFIS control.

V. CONCLUSION

In this paper, an analytical investigation of a new swimming microrobot device and its control strategy have been proposed. The analytical analysis has been developed in order to calculate the microrobot performances, which are: the velocity and the total thrust force. The thrust force, the velocity and microrobot geometry are considered as important parameters for high controllability and reliability performances. The proposed design and control strategy have been shown a high electromechanical performance in comparison to the conventional structures. Moreover, the applicability of the ANFIS-Flatness-based approach for the improvement of the swimming microrobot design and its controllability has been proved in this study. It can be concluded that the proposed ANFIS-Flatness-based control is an efficient tool for high performance microrobot-based applications.

REFERENCES

[1] X. Chang, L. Zhang, X. He, "Numerical study of the thunniform mode of fish swimming with different Reynolds number and caudal fin shape," J. Computers & Fluids, Vol. 68, pp. 54–70, 2012.

[2] Y. Liu, G. Sun and H. Chen, "A Micro Robot with the Ability of Fly and Adhesion:Development and Experiment," in: Procedings of the 2011 IEEE-International Conference Robotics and Biomimetics, Phuket, Thailand, 2011.

[3] S. P. Woods and T.G. Constandinou, "Wireless Capsule Endoscope for Targeted Drug Delivery: Mechanics and Design Considerations," IEEE Trans on nanobioscience, Vol. 60, pp. 945-953, 2013.

[4] H. Horiguchi, K. Imagawa, T. Hoshino, "Fabrication and Evaluation of Reconstructed Cardiac Tissue and Its Application to Bio-actuated Microdevices," IEEE Trans on nanobioscience, Vol. 8, pp. 349-359, 2009.

[5] L. Arcese, M. Fruchard, and A. Ferreira, "Endovascular Magnetically Guided Robots: Navigation Modeling and Optimization," IEEE Trans on Biomedical Engineering , Vol. 59, pp. 977-987, 2012.

[6] F. Srairi, M. Meguellati, L. Saidi and F. Djeffal, "Analytical Modeling and Optimization of New Swimming Microrobot design using genetic algorithm computations," 14th IEEE International conference on Sciences and Techniques of Automatic control & computer engineering, STA'2013, pp. 265-268, Sousse, Tunisia, 2013.

[7] F. Djeffal, D. Arar, N. Abdelmalek, M.A. Abdi, R. Mahamdi, A. Errachid, "A junctionless-multigate design to improve the electrical performances for deep submicron ISFET-based sensors," Sensor Letters, Vol. 9, pp. 2309-2311, 2011.

[8] T. Bendib, F. Djeffal, M. A. Abdi, D. Arar, "An Analytical analysis of the sensitivity behaviour for deep submicron ISFET sensors," Third International Conference Electrical Engineering Design, ICEEDT09, Sousse, Tunisia, 2009.

[9] M. Meguellati, F. Djeffal, D. Arar, F. Douak and L. Khettache, "New RADFET Dosimeter Design For Radioactive Environment Monitoring Applications," Eng Lett, Vol. 20, EL 20-4-06, 2012.

[10] M. Meguellati, F. Djeffal, "New Dual-Dielectric Gate All Around (DDGAA) RADFET dosimeter design to improve the radiation sensitivity," Nuc Instr and Meth in Phys Res, Vol. A 683 pp. 24-28, 2012.

[11] D. Arar , F. Djeffal , T. Bentrcia, M. Chahdi, "New junctionless RADFET dosimeter design for low-cost radiation monitoring applications," Physica Status Solidi (C) Current Topics in Solid State Physics Vol. 11, pp. 65-68, 2014.

[12] F. Djeffal, M. Meguellati, "Multigate RADFET dosimeter for radioactive environment monitoring applications," Lecture Notes in Electrical Engineering (LNEE), Vol. 229, pp. 301-313, 2013.

[13] M. Meguellati, F. Djeffal, D. Arar, T. Bendib, L. Khettache, "RADFET dosimeter design for environment monitoring applications," Proceedings of the International Conference on Microelectronics, ICM'2012, Algiers, Algeria, pp. 1-4, 2012.

[14] Dennis E. Curtin, Robert D. Lousenberg, Timothy J. Henry, Paul C. Tangeman, Monica E. Tisack "Advanced materials for improved PEMFC performance and life," Journal of Power Sources Vol. 131, pp. 41-8, 2004. .

[15] T. Bentrcia, F. Djeffal, D. Arar, M. Meguellati, "ANFIS-based computation to study the nanoscale circuit including the hot-carrier and quantum confinement," The 5th International Conference on Modeling, Simulation and Applied Optimization, pp. 1-5, 2013.

[16] T. Bentrcia, F. Djeffal, E. Chebaaki, "ANFIS-based approach to study the subthreshold swing behavior for nanoscale DG MOSFETs including the interface trap effect," The 24th International Conference on Microelectronics, pp.1-4, 2012.

[17] J. Jang, "ANFIS: adaptive-network-based fuzzy inference system," J. IEEE Transactions on Systems Man and Cybernytics, Vol. 23, pp. 665–685, 1993.

[18] F. Djeffal, S. Guessasma, A. Benhaya, M. Chahdi, "An analytical approach based on neural computation to estimate the lifetime of deep submicron MOSFETs," Journal of Semiconductor Science and Technology, Vol. 20, pp. 158-164, 2005.

[19] L. Arcese, F. Matthieu, B. Felix, A. Ferreira, B. J. Nelson, " Adaptive Controller and Observer for a Magnetic Microrobot," IEEE Transactions on Robotics, Vol. 29, pp. 1060-1067, 2013.